

Supplemental Material

Oceanic intraplate faulting as a pathway for deep lithosphere hydration: Perspectives from the Caribbean

Brandon T. Bishop¹, Sungwon Cho¹, Linda Warren¹, Lillian Soto-Cordero¹, Patricia Pedraza², German A. Prieto³, Viviana Dionicio²

¹Department of Earth and Atmospheric Sciences, Saint Louis University, 3642 Lindell Blvd, St. Louis, Missouri 63108, USA

²Red Sismológica Nacional de Colombia, Servicio Geológico Colombiano, Diagonal 53 # 34-53, Bogotá D.C., Colombia

³Departamento de Geociencias, Universidad Nacional de Colombia, Av. Carrera 30 # 45-03, Bogotá D.C., Colombia

In the first section, we provide a simplified version of Fig. 1 with the labeled station locations used in our study. In the subsequent four sections, we show HypoDD (Waldhauser and Ellsworth, 2000) relocation results for the Providencia sequence of earthquakes calculated using the data described within the main text's Data section and the velocity models described in Table 2 but not shown in the main text. Discussion of these results may be found in the main text's Effects of Velocity Model on Event Relocation and Effects of Moho Depth sections. In the second section, we examine the effects of an overestimated or underestimated Mohorovičić Discontinuity (Moho) depth on the relocation of events located immediately above and below the Moho. In the third section, we present a Hk-plot for station PRV and discuss the limitations of its use for assessing crustal thickness and Vp/Vs. Finally, we note that the earthquake relocations for the Providencia sequence are available as a Table S3 in a separate supplemental file, GS2534_TabS3.xlsx.

MAP WITH LABELED STATION LOCATIONS

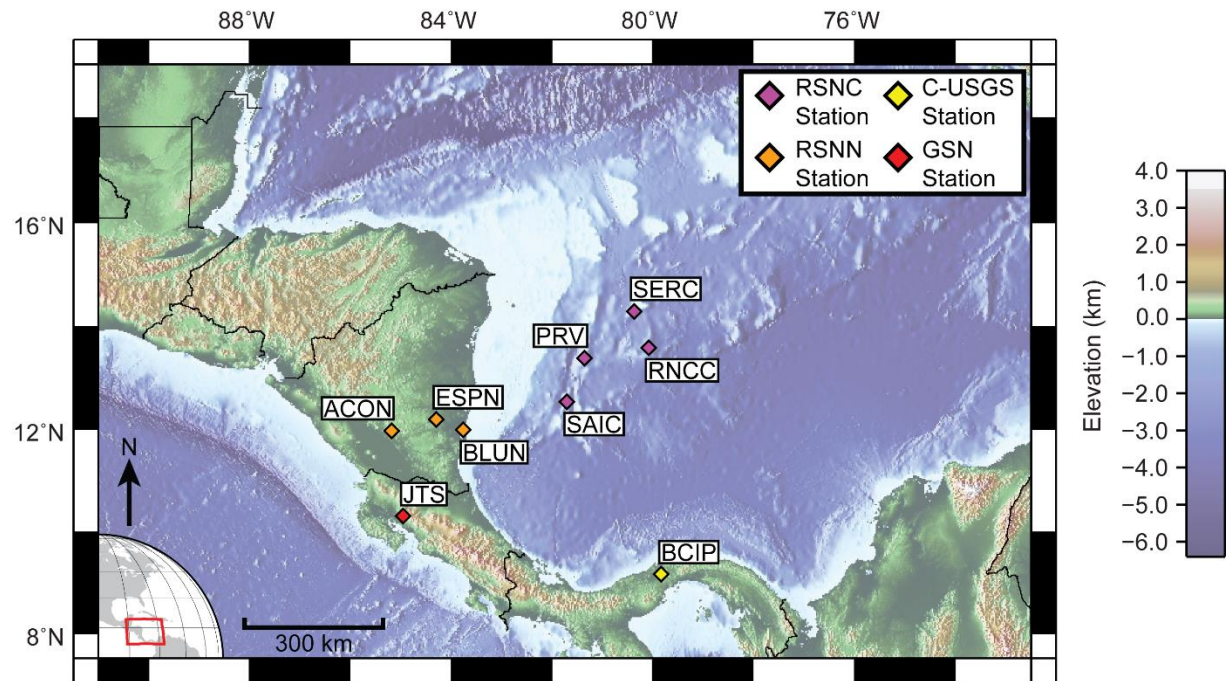


Figure S1. Map of stations used in the study. See Fig. 1 in the main text for tectonic features.

MODELS WITH VARYING SEDIMENT LAYER THICKNESS

The elevation of the Providencia region lies mostly at depths between 1 and 2 km below sea level on the Lower Nicaragua Rise (Fig. 1A,B). The overall thickness of sedimentary units in the region is also somewhat variable, as documented in active source seismic studies (e.g. Mauffret and Leroy, 1997; Carvajal-Arenas et al., 2015; Carvajal-Arenas and Mann, 2018). Generally, these units are a combined ~0.5-1.5 km in thickness. The upper layer of our velocity models must account for both bathymetry of the region and the thickness of sedimentary units as HypoDD does not permit variable or negative topography. As such, we try velocity models with a 2.5 km, 3 km, and 3.5 km thick top layer with a P-wave speed of 2.40 km/s typical of sedimentary units in the region.

Fig. S2A shows the relocations obtained using the 2.5 km thick layer model; Fig. S2B shows those obtained using the 3.0 km thick layer model; and Fig. S2C shows the results obtained using our preferred 3.5 km thick layer model. See the main text's Effects of Velocity Model on Event Relocation section for further discussion.

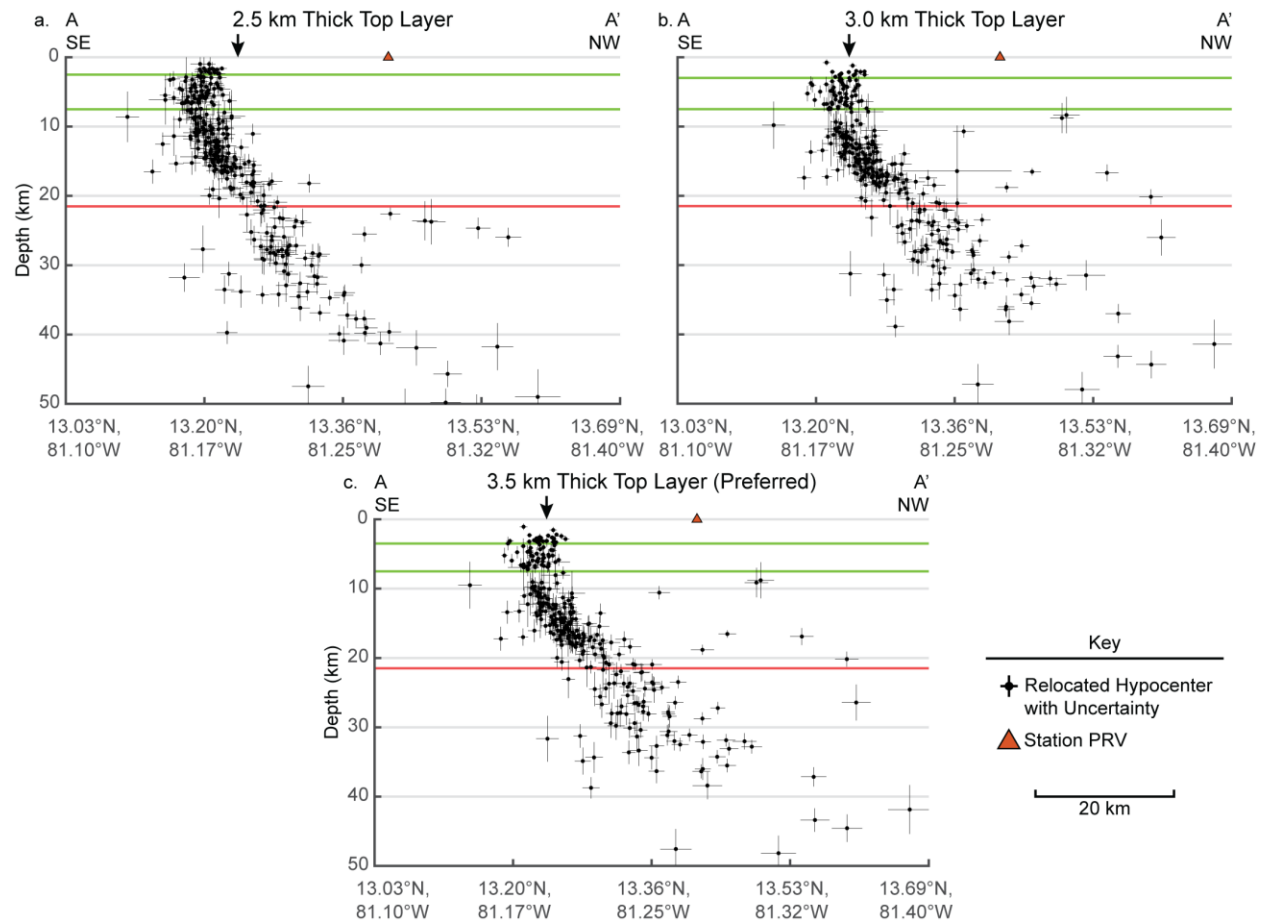


Figure S2. Effects of varying sedimentary layer thickness along cross-section A-A' (see Fig. 1).

MODELS WITHOUT A SEDIMENTARY LAYER, VARYING OCEANIC LAYER 2,3 THICKNESS

Results from the previous section suggest that our data set is not strongly influenced by the thickness of the shallowest sedimentary layer. To investigate this further, we calculated results using two alternate models that remove the sedimentary layer. In order to maintain crustal

thickness, we must add 3.5 km to either Oceanic Layer 2 or Oceanic Layer 3. Oceanic Layer 2 for the Providencia region has a P-wave velocity of ~ 5.25 km/s while Oceanic Layer 3 has a P-wave velocity of 7.00 km/s (Mauffret & Leroy, 1997).

Fig. S3A shows the relocations calculated using the thicker Oceanic Layer 2 model; Fig. S3B shows those calculated using the thicker Oceanic Layer 3 model; and Fig. S3C again shows relocations calculated using our preferred model for reference. See main text's Effects of Velocity Model on Event Relocation section for further discussion.

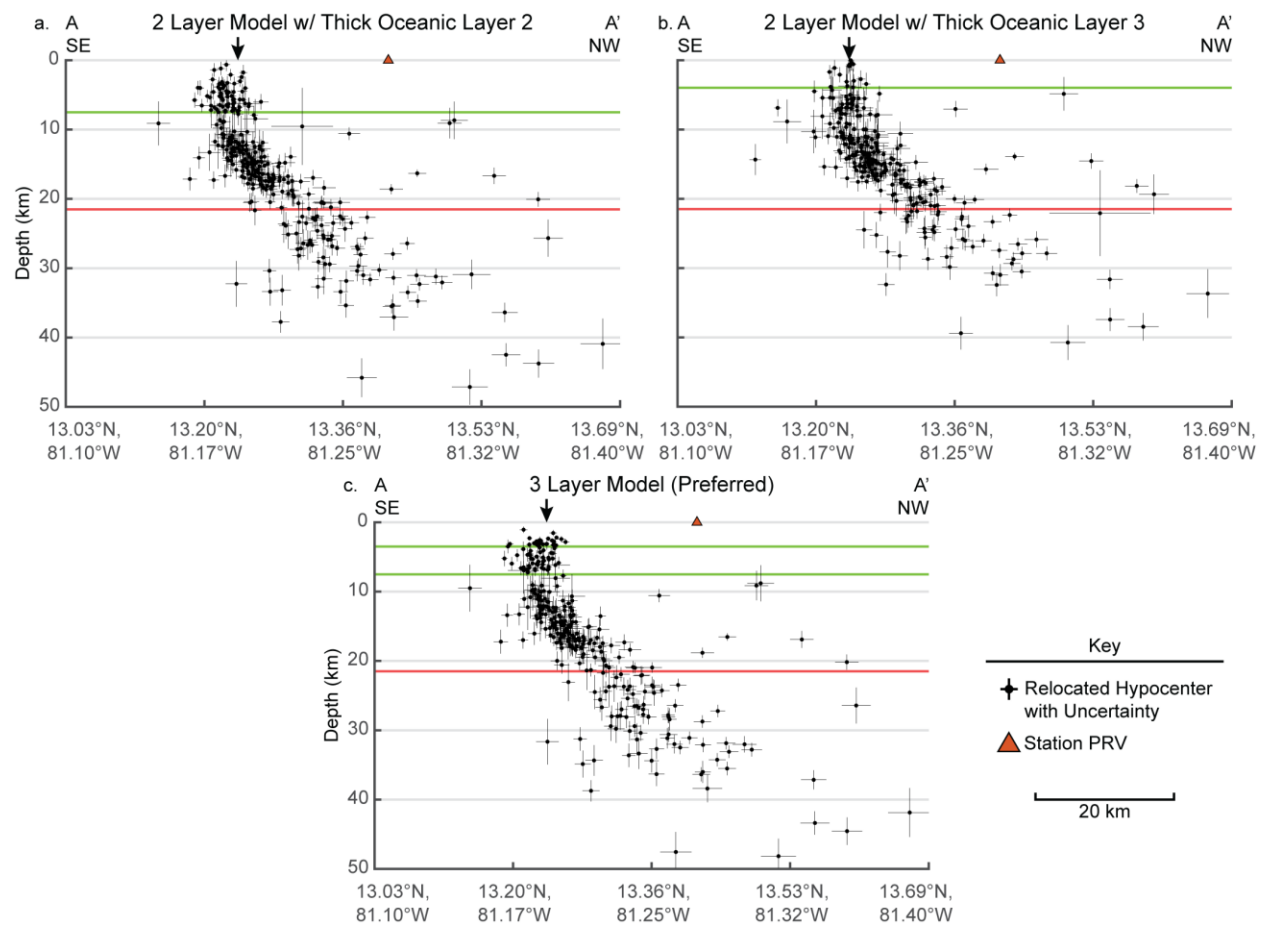


Figure S3. Effects of removing the sediment layer and thickening other layers along cross-section A-A' (see Fig. 1).

MODELS WITH ALTERNATE OCEANIC LAYER 3 VELOCITIES

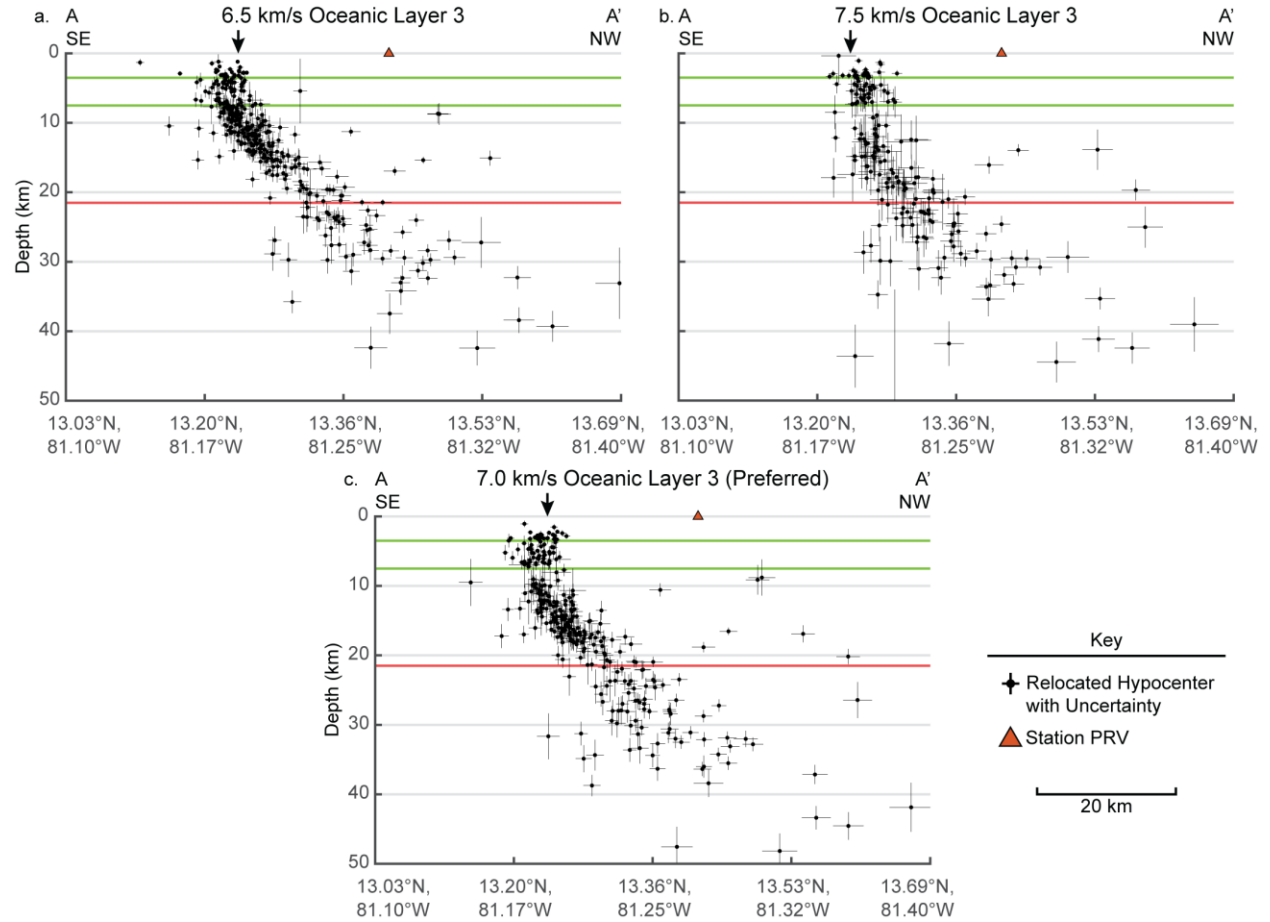


Figure S4. Effects of altering Oceanic Layer 3 velocity along cross-section A-A' (see Fig. 1).

Our results from the second section above suggest that Oceanic Layer 3 may have a comparatively influential role on our relocations. To investigate this further, we use two models with alternate P-wave velocities for Oceanic Layer 3 that fall within the range of values reported for the Caribbean region by Mauffret & Leroy (1997). The first model is assigned an Oceanic Layer 3 P-wave velocity of 6.50 km/s while the second is assigned a velocity of 7.50 km/s.

Fig. S4A shows the relocations we obtain using the slower Oceanic Layer 3 model; Fig. S4B shows those obtained using the faster Oceanic Layer 3 model; once again Fig. S4C shows

relocations obtained using our preferred model. See main text's Effects of Velocity Model on Event Relocation section for additional discussion.

MODEL OF EXTENDED CONTINENTAL CRUST

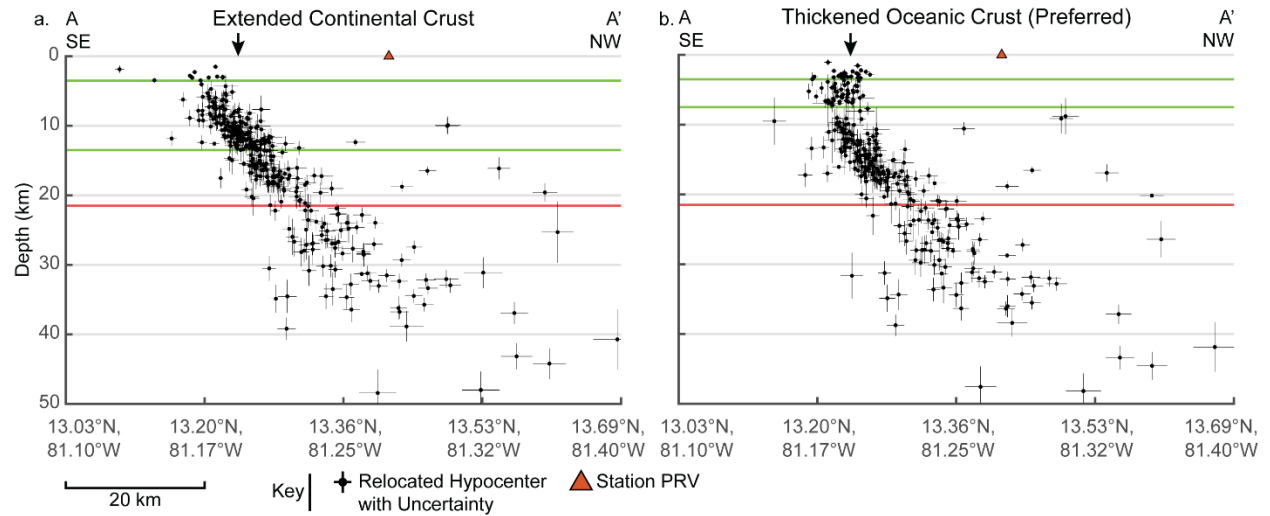


Figure S5. Effects of using an extended continental crust model along cross-section A-A' (see Fig. 1).

The relatively low average uncertainties obtained from the slower 6.5 km/s Oceanic Layer 3 model above suggests that a velocity model based on Carvajal-Arenas and Mann (2018)'s interpretation of the Lower Nicaragua Rise as extended continental crust may be appropriate for our study area. To test this, we created a model with a 6.0 km/s upper layer corresponding to the 2.7 g/cm³ material (typical of felsic rocks) from Carvajal-Arenas and Mann (2018) and a 7.0 km/s lower layer corresponding to the 2.9 g/cm³ material (typical of mafic rocks) used by the same study.

Fig. S5A shows the relocations we obtained using the extended continental crust model; Fig. S5B shows the relocations obtained using our preferred model. See main text's Effects of Velocity Model on Event Relocation for additional discussion.

MODELS WITH ALTERNATE Vp/Vs VALUES

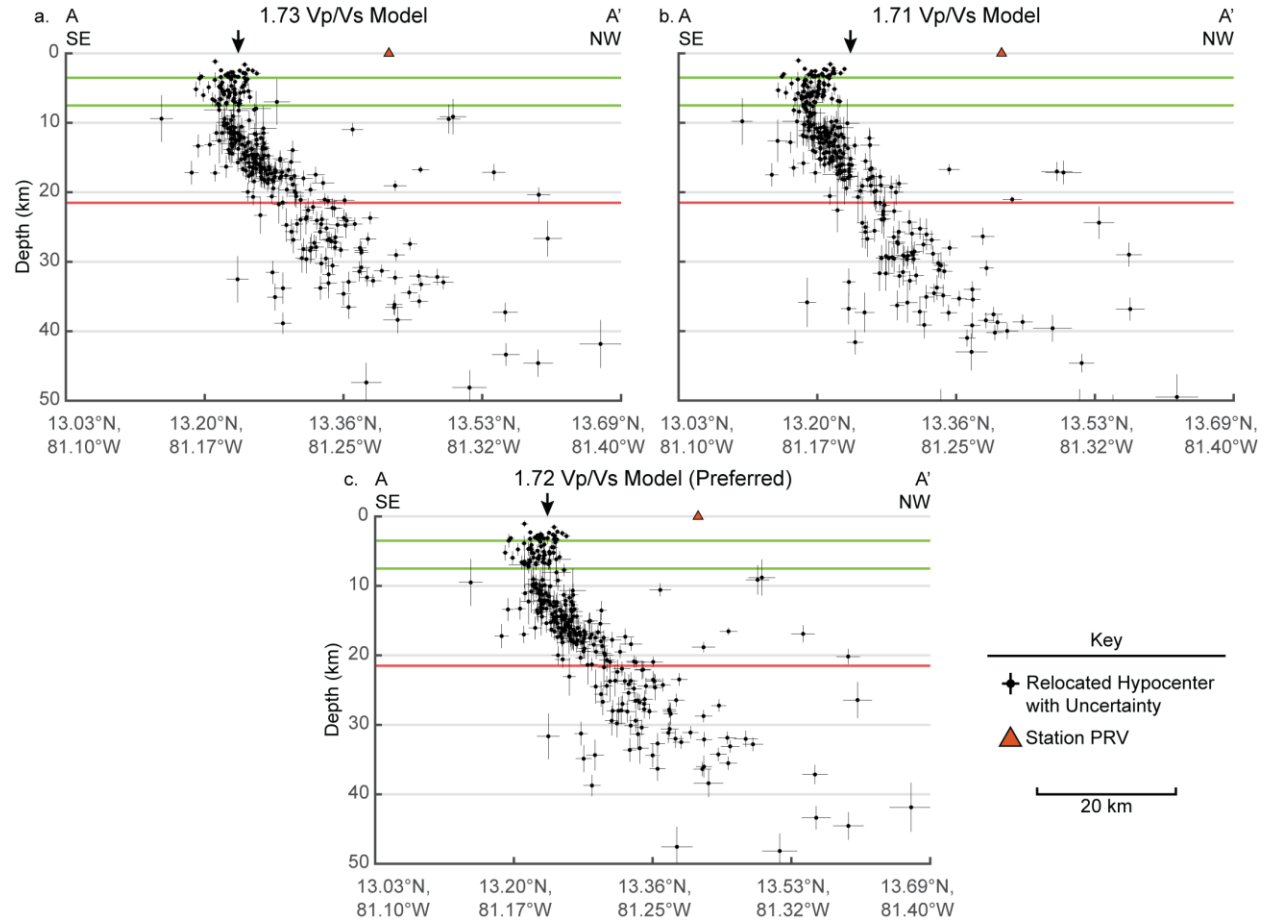


Figure S6. Effects of altering the Vp/Vs value along cross-section A-A' (see Fig. 1).

As discussed in the main text, we calculated the regional Vp/Vs value for the Providencia region using a bootstrapped Wadati Plot. This provided a Vp/Vs value of 1.72 and a 2- σ uncertainty of ± 0.01 . This range is within the expected range for peridotite compositions at uppermost mantle pressures and temperatures (Abers & Hacker, 2016), consistent with the ray paths to our stations passing mostly through the mantle. We used models with the high and low Vp/Vs values permitted by our Wadati Plot calculation to examine possible changes to our relocations.

Fig. S6A shows the relocations calculated using the high 1.73 Vp/Vs model; Fig. S6B shows those calculated using the low 1.71 Vp/Vs model; Fig S6C provides relocations calculated using our preferred Vp/Vs value of 1.72 as a point of reference. See main text's Effects of Velocity Model on Event Relocation section for additional discussion.

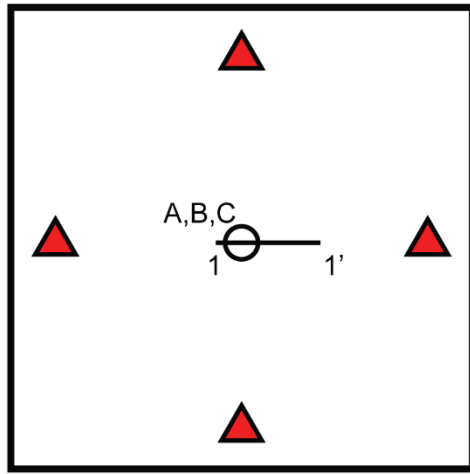
CONSIDERATION OF THE EFFECTS OF AN UNDER- OR OVERESTIMATED MOHO DEPTH

Our focus here is developing first-order intuition for the behavior of HypoDD (Waldhauser & Ellsworth, 2000) and other double-difference approaches to earthquake relocation when a set of earthquakes occurs across a strong, relatively flat velocity contrast. Two settings are likely to produce such a configuration: 1) extremely shallow events occurring across the contact between sedimentary units and the crystalline basement; 2) deep crustal events occurring across the Moho separating the crust and mantle. We leave aside the first of these as being well beyond the scope of our current study given our sparse station distribution and note that the second of these is unlikely occur outside of an ocean basin in which the lithosphere is relatively old and may have brittle behavior within the plate's mantle (e.g. Kwong et al. 2019 and the results we present within the main text of the present study). We also note that this case is not likely to hold for events cutting across a subducted oceanic Moho as the dip of the subducting plate will significantly affect ray paths. A rigorous, generalized exploration of this behavior is beyond the scope of the present work.

We begin by recognizing that the results we have obtained for differing estimates of the oceanic Moho in the Providencia region produce a clear trend in relocation results (Fig. 4). Models in which the Moho is at <21.5 km depth exhibit a relatively earthquake free patch up to ~2 km above and below the modeled Moho depth. Models with a Moho depth ≥ 21.5 km do not

show this patch. This behavior appears distinct from the behavior sometimes observed in non-double-difference earthquake location approaches which tends to collect events along sharp velocity model boundaries (e.g. results for non-gradational boundaries in Lomax, 2020). It also differs significantly in behavior from the smaller-scale flattening artifacts that may be observed away from layer boundaries explored by Michelini & Lomax (2004) using a double-difference approach. Given that this pathology is limited to the vicinity of a layer boundary, we expect the behavior to be related to the way in which errors in ray pathing interact with the double-difference approach.

Fig. S7 provides a geometrically correct representation of the P-wave ray paths for three events occurring at the same X and Y position but at differing depths. In both the under- and overestimated cases shown in Fig. S7, event A occurs within the crustal layer while event C occurs within the mantle half-space. Event B occurs within the lower 2.5 km of the crustal layer for the underestimated Moho depth case and within the upper 2.5 km of the mantle half-space in the overestimated case. Our arbitrary configuration of four stations located at 90° intervals around and equidistant from the 3 events is used to further simplify the problem. A movement laterally towards any one station would introduce a counteracting misfit at the opposite station, and we assume a heavy penalty has been applied for any such misfit.



Stations equidistant from events A,B,C.
Stations at a distance such that first arrival for event A is Pn.

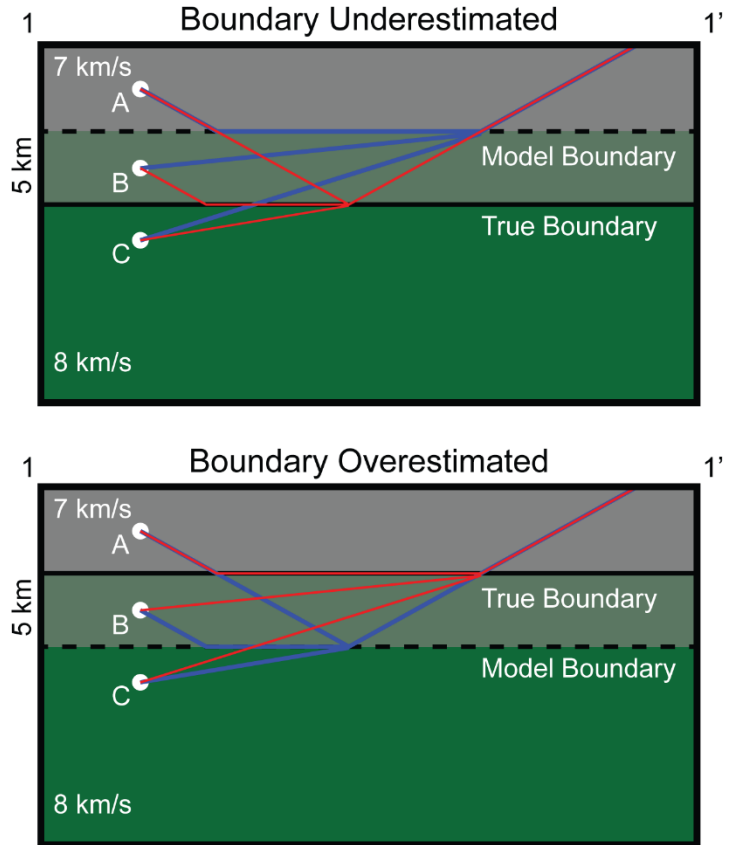


Figure S7. Difference in true ray path (red) and initially estimated ray path (blue) for three events vertically offset from each other by 5 km. Here we consider the sets of ray paths arriving only at the right station of the four station array; in cross-section view, paths to other stations would be rotated by 90° but otherwise appear identical.

Travel-times along shared ray paths are eliminated in double difference approaches, and we exploit this to simplify our calculations. We consider only the parts of the ray paths which are not shared by either the true ray paths (red lines) or the modeled ray paths (blue lines) and present them and their corresponding travel-time differentials in Tables S1 and S2, below.

TABLE S1. RAY GEOMETRIES

Ray Path	Event Name	Distance in crustal layer (km)	Distance in mantle halfspace (km)	Time taken (s)
<u>Underestimated Moho Depth, True Ray Path</u>				
	A	15.4700	0.0000	2.2100
	B	5.1567	9.0292	1.8653
	C	0.0000	13.7594	1.7199
<u>Underestimated Moho Depth, Modeled Ray Path</u>				
	A	5.1567	18.0440	2.9922
	B	0.0000	22.6888	2.8361
	C	0.0000	23.7651	2.9706
<u>Overestimated Moho Depth, True Ray Path</u>				
	A	5.1567	18.0440	2.9922
	B	0.0000	22.6886	2.8361
	C	0.0000	23.7651	2.9706
<u>Overestimated Moho Depth, Modeled Ray Path</u>				
	A	15.4700	0.0000	2.2100
	B	5.1567	9.0292	1.8653
	C	0.0000	13.7594	1.7199

TABLE S2. TRAVEL-TIME DIFFERENTIALS

Set of Ray Path	Event Pair	Travel-Time Differential (s)
<u>Underestimated Moho Depth, True Ray Paths</u>		
	A-B	0.3447
	B-C	0.1444
	A-C	0.4901
<u>Underestimated Moho Depth, Modeled Ray Paths</u>		
	A-B	0.1561
	B-C	-0.1345
	A-C	0.0216
<u>Overestimated Moho Depth, True Ray Paths</u>		
	A-B	0.1561
	B-C	-0.1345
	A-C	0.0216
<u>Overestimated Moho Depth, Modeled Ray Paths</u>		
	A-B	0.3447
	B-C	0.1444
	A-C	0.4901

In the underestimated Moho case, the relocation program will attempt to increase all three modeled travel-time differentials. This may be accomplished most easily by moving event A

upward, increasing the length of the ray path in the overlying slow crustal layer. Event B will likewise be moved downward in an attempt to increase the value of the modeled B-C term—however our station geometry will impose a tradeoff for other modeled terms. In a case allowing lateral movement, the modelled B-C term would likely increase by lateral displacement of event B away from the majority of stations and towards a somewhat greater depth. The magnitude of this displacement will decrease for cases where event B occurs closer to the depth of event C. The overall effect of an underestimated Moho will tend to force events which plot above the modelled Moho upwards, while displacing events above the true Moho but below the modeled Moho to greater depth.

In the overestimated case, relocation will attempt to decrease all three travel-time differentials. This may be accomplished by increasing the depth of events A and B while decreasing the depth of C. In this case, the three differentials may allow event C to move to a depth shallower than event B. This effect will be most pronounced for events directly below the true Moho. These trends will tend to cause events occurring around an overestimated Moho depth to be drawn closer the modelled Moho.

For a cluster of events distributed over a relatively wide range of depths above and below the Moho, the underestimated case will tend to be a more obvious artifact than the overestimated case. This is due to the underestimated Moho case producing a discrete gap in the relocated events. This behavior would not be expected for most geologically reasonable pressure-temperature-composition configurations and is visually conspicuous. The overestimated Moho case will tend to create a clump of seismicity near the modelled Moho, which could be interpreted as a localized concentration of seismicity rather than an artifact of the double-difference approach.

For larger station event offsets, the observed effect is likely to hold as the differences between event pair paths remain similar to those shown in Fig. S7. For smaller station offsets, the effect should reduce to a more conventional tradeoff in event depth and origin time as the model's calculated direct arrival begins to coincide with the geometry for the true direct arrival with only a slight deflection at the Moho.

Larger, more spatially complex sets of events recorded at stations with an uneven distribution will complicate the patterns described here. The general tendency of events to be displaced from an underestimated Moho and attracted towards an overestimated Moho would likely tradeoff with lateral displacements and changes in estimated origin time, somewhat diminishing vertical effects we discuss here.

HK-PLOT FOR STATION PRV

Receiver functions can be used to estimate the tradeoff between crustal thickness (H) and crustal V_p/V_s ratio (κ) through $H\kappa$ -stacking (Zhu and Kanamori, 2000). The $H\kappa$ -stacking technique is essentially a grid search: for an assumed value of V_p and a set of receiver functions with known ray parameters (ultimately a measure of the angle of incidence), a search of times corresponding to the arrival times of an interface's converted P_s phase and its first and second multiples (reverberations between the Earth's surface and the interface) predicted according to a range of H and κ values. The amplitude of the receiver functions at each of these times is summed after correcting for each receiver function's ray parameter and the second multiples' polarity reversals. The highest value should correspond to the true H and κ .

Success of the $H\kappa$ -stacking approach requires that the Earth's structure beneath a seismic station be relatively uniform and simple (see discussion in Frassetto et al., 2011 and references

therein). Significant azimuthal variation in crustal composition, a dipping interface, or anisotropy will move arrivals away from the modeled arrival times. The presence of additional interfaces above or below the Moho and their multiples may constructively or destructively interfere, altering the amplitudes measured by the stack. This has often led receiver function studies to augment their analysis by calculating V_p/V_s via Wadati plots for stations in areas of geologic complexity (e.g., Frassetto et al., 2011; Poveda et al., 2015).

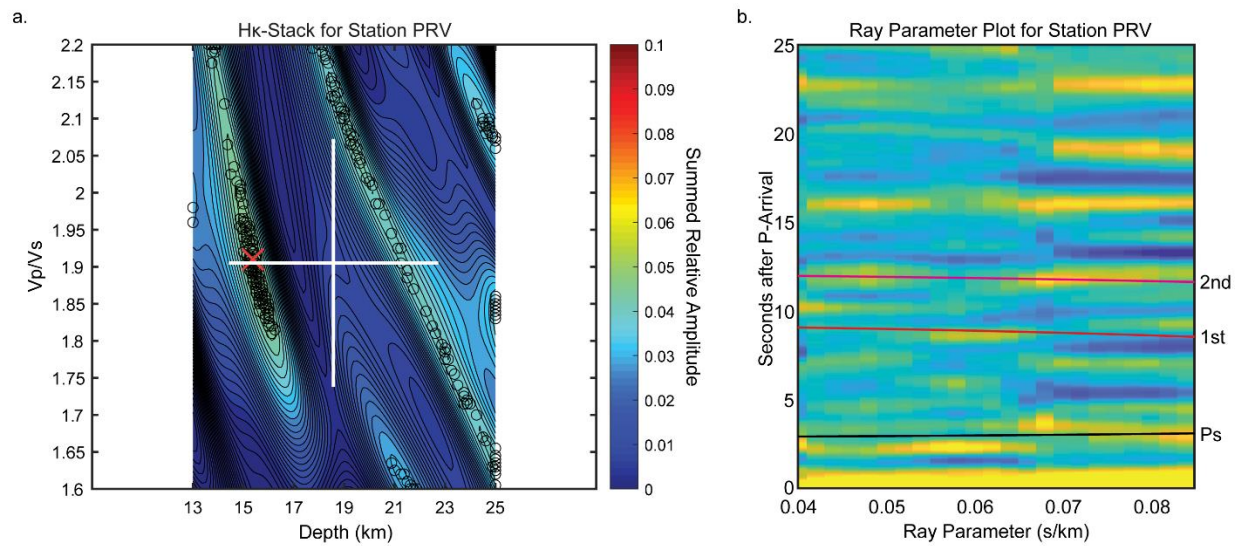


Figure S8. (A) Hk-plot for station PRV assuming a V_p of 6.0 km/s. Ps and 1st multiple arrivals have been assigned an equal weight for the stack and 2nd multiples have been assigned a weighting half of the other phases. Black circles mark highest value found for individual bootstraps. White cross marks 1- σ uncertainty for V_p/V_s and Moho depth. Red “x” marks global maximum of the summed relative amplitudes. (B) Predicted curves for Moho Ps arrival and it’s 1st and 2nd multiples assuming the V_p/V_s (1.91) and Moho depth (18.6 km) found from the Hk-stack are correct. Background color marks receiver function polarity (yellow is positive, blue is negative).

Fig. S8 shows the results of Hk-stacking for station PRV. Possible V_p/V_s values have been restricted to realistic values for rock or for rock containing a fluid component. Depth values

are restricted to those reported by prior studies of the Lower Nicaragua Rise. The nominal estimate of V_p/V_s for the station is 1.91 with a 1- σ uncertainty of ± 0.17 and the nominal estimate for Moho depth is 18.6 with a 1- σ uncertainty of ± 8.4 km. Visual inspection of Fig. S8A clearly indicates that these estimates are not an accurate estimate of either value. No single, prominent value or range of values can be identified on the plot. Examination of Fig. S8B indicates that the estimates from the Hk-stack are strongly influenced by the Ps arrival at 2-3 seconds, but little constraint is supplied by the multiples.

These results are consistent with our interpretation in the main text of the velocity structure beneath PRV being highly complex. See the main text's Receiver Functions From Station PRV on Isla Providencia section for discussion of this complexity and its significance.

REFERENCES CITED

- Abers, G.A., and Hacker, B.R., A MATLAB toolbox and Excel workbook for calculating the densities, seismic wave speeds, and major element composition of minerals and rocks at pressure and temperature: *Geochemistry, Geophysics, Geosystems*, v. 17, p. 616-624, doi:10.1002/2015GC006171.
- Carvajal-Arenas, L.C., Torrado, L., and Mann, P., 2015, Early and late Eocene/Oligo-Miocene (!) petroleum system on the Nicaraguan Rise: Insights from basin and three-dimensional petroleum system modeling, *in* Bartolini, C., and Mann, P., eds., *Petroleum Geology and Potential of the Colombian Caribbean Margin: American Association of Petroleum Geologists Memoir 108*, p. 615-646, doi:10.1306/13531951M1083654.
- Carvajal-Arenas, L.C., and Mann, P., 2018: Western Caribbean intraplate deformation: defining a continuous and active microplate boundary along the San Andres rift and Hess

- Escarpment fault zone, Colombian Caribbean Sea: AAPG Bull., v. 102, p. 1523-1563, doi:10.1306/12081717221.
- Frassetto, A.M., Zandt, G., Gilbert, H., Owens, T.J., and Jones, C.H., 2011, Structure of the Sierra Nevada from receiver functions and implications for lithospheric foundering: Geosphere, v. 7, n. 4, p. 898-912, doi:10.1130/GES00570.1.
- Kwong, K.B., Deshon, H.R., Saul, J., and Thurber, C.H., 2019, Constraining the oceanic lithosphere seismogenic zone using teleseismic relocations of the 2012 Wharton Basin great earthquake sequence: Journal of Geophysical Research Solid Earth: v. 124, p. 11,938-11,950, doi:10.1029/2019JB017549.
- Lomax, A., 2020, Absolute location of 2019 Ridgecrest seismicity reveals a shallow M_w 7.1 hypocenter, migration and pulsing M_w 7.1 foreshocks, and duplex M_w 6.4 ruptures: Bulletin of the Seismological Society of America, v. 110, p. 1845-1858, doi:10.1785/0120200006.
- Mauffret, A., and Leroy, S., 1997, Seismic stratigraphy and structure of the Caribbean igneous province: Tectonophysics, v. 283, p. 61-104, doi:10.1016/S0040-1951(97)00103-0.
- Michellini, A., and Lomax, A., 2004, The effect of velocity structure errors on double-difference earthquake location: Geophysical Research Letters, v. 31, L09602, doi:10.1029/2004GL019682.
- Poveda, E., Monsalve, G., and Vargas, C.A., 2015, Receiver functions and crustal structure of the northwestern Andean region, Colombia: Journal of Geophysical Research Solid Earth, v. 120, p. 2408-2425, doi:10.1002/2014JB011304.
- Waldhauser, F., and Ellsworth, W.L., 2000, A double-difference earthquake location algorithm: Method and application on the northern Hayward Fault, California: Bulletin of the Seismological Society of America, v. 90, p. 1353-1368, doi:10.1785/0120000006.

Zhu, L., and Kanamori, H., 2000, Moho depth variation in southern California from teleseismic receiver functions: *Journal of Geophysical Research Solid Earth*, v. 105, p. 2969-2980, doi:10.1029/1999JB900322.